Supporting Information

Towards high-performance nonlinear optical through embedding D-A system into β-ketoenamine-linked COFs

Mingyan Li [a], Jiahui Chu [a], Debo Ding [a], Tingting Li [a], Endian Su [a], Yinglin Song [b], Yun-Fang Yang [a], Yuanbin She [a,], and Jianhong Jia [a,*]*

[a] College of Chemical Engineering, Zhejiang University of Technology, Hangzhou 310014, China, E-mail: zgdjjh@163.com (J. Jia); sheyb@zjut.edu.cn (Y. She)

[b] School of Physical Science and Technology, Soochow University, Suzhou 215123, China

Experimental Section

1. Material

1,3,5-Triformylbenzene (TF) and 2,4,6-trihydroxybenzene-1,3,5-trialdehyde (TFP) were purchased from BIDE PHARMATECH CO., LTD. Tetrahydrofuran (THF), *o*-dichlorobenzene (*o*-DCB), *n*-butyl alcohol (*n*-BuOH), acetic acid, N,N-dimethylacetamide (DMAC), and acetone were purchased from chemical reagent manufacturers. Glass blocks (NeVid S27105) with dimensions of 25.0 × 75.0 mm and thickness of 1.0 ~ 1.2 mm were used. Before use, they were cut into rectangles of size 1.0 × 0.8 cm using a glass knife. The N_4,N_4-bis(4'-amino-[1,1'-biphenyl]-4-yl)-[1,1'-biphenyl-4,4'-diamin] (BABD) used in this study was from the same batch as those reported by Li *et al.* and further characterization can be found therein.[1] With the exception of BABD, all chemicals utilized in this study were obtained commercially and employed without further purification.

2. Experimental Section

2.1. Preparation of TF-BD Powder and Film

N_4,N_4-bis(4'-amino-[1,1'-biphenyl]-4-yl)-[1,1'-biphenyl-4,4'-diamin] (BABD,40.0 mg, 0.0771 mmol) and 1,3,5-triformylbenzene (TF, 12.5 mg, 0.0771 mmol) was successively added into 5 mL glass bottles. Subsequently, 1.25 mL of *o*-dichlorobenzene (*o*-DCB) and 1.25 mL of *n*-butanol (*n*-BuOH) were added, and the resulting mixture was ultrasound treated for 5 minutes. Next, the pre-treated glass sheets were added to the mixture, and the entire mixture was transferred to a 25 mL glass ampere bottle along with the glass sheets. Additionally, 0.25 mL of 6 M acetic acid was added to the mixture. Following this, the mixture was sealed and subjected to three freezing-vacuum-thawing cycles at a temperature of 77 K liquid nitrogen. Subsequently, it was heated at a temperature of 120 ℃ for a duration of 5 days. Once the reaction had cooled to room temperature, the glass sheet was cleaned using N,N-dimethylacetamide (DMAC) and acetone to obtain the TF-BD film. The remaining solids were washed three times using DMAC and acetone filtration. The obtained powder was extracted by Soxhlet extraction with THF and acetone acted as detergents for 48 h. Finally, TF-BD was obtained as a yellow powder after undergoing vacuum activation at a temperature of 90 ℃ for 24 hours.

2.2. Preparation of TFP-BD Powder and Film

A 5 mL glass bottle was used to combine BABD (36.9 mg, 0.0711 mmol) and 2,4,6-triformylphloroglucinol (TFP, 15.0 mg, 0.0711 mmol) with 1.5 mL of *o*-DCB and 1.5 mL of *n*-BuOH. Ultrasound treatment was applied to the mixture for 5 minutes. Subsequently, the pre-treated glass sheets were added to the mixture, and the entire mixture was transferred to a 25 mL glass ampere bottle along with the glass sheets. Additionally, 0.30 mL of 6 M acetic acid was added to the mixture. Following this, the mixture was sealed and subjected to three freezing-vacuum-thawing cycles at a temperature of 77 K liquid nitrogen. Next, the reaction was heated at 120 ℃ for 3 days. After cooling to room temperature, the glass sheet was washed with DMAC and acetone to obtain the TFP-BD film. The residual solution from the reaction system was filtered, and the resulting solids were washed three times with DMAC and acetone. The obtained powder was Soxhlet extraction with THF and acetone acted as detergents for 48 hours. Finally, the yellow powder of TFP-BD was obtained after vacuum activation at 90 ℃ for 24 hours.

3. Characterization

Power X-ray diffraction (PXRD) patterns were collected using a Cu Kα radiation X-ray diffraction system (DX-27mini, China). Fourier transform infrared (FT-IR) spectra were measured using an IR spectrometer (Nicolet 6700) in the ranges of 4000 to 400 cm^{-1}. X-ray Photoelectron Spectroscopy (XPS) was performed on a Thermo Scientific K-Alpha XPS system equipped with a monochromatic Al Kα X-ray source (hv = 1486.6 eV). The binding energies in all obtained XPS spectra were calibrated using the C 1s peak at 284.8 eV. Solid-state NMR spectra were acquired using a Bruker 400M spectrometer with cross-polarization magic-angle-spinning (CP/MAS) at a resonance frequency of 150.9 MHz. ^{13}C CP/MAS NMR spectra were recorded using a 4 mm MAS probe and a spinning rate of 10 kHz. A contact time of 4 s and a recycle delay of 6.5 μs were used for the ^{13}C CP/MAS NMR measurement. The chemical shifts of ^{13}C were externally referenced to tetramethylsilane (TMS). Scanning electron microscopy (SEM) images were obtained using a GeminiSEM 500 system. Transmission electron microscopy (TEM) images were acquired using a Tecnai G2 F30 S-Twin. Thermogravimetric analysis (TGA) was performed using a NETZSCH TG 209 F1 Libra under flowing N_2 with a ramp rate of 20 K min^{-1}. The Brunauer-Emmett-Teller (BET) surface areas were calculated from N_2

sorption isotherms at 77 K using a Micromeritics ASAP 2460 3.01 system surface area and pore size analyzer. Solid-state ultraviolet-visible (UV-Vis) absorption of the sample was recorded using the Shimadzu UV-2600i UV-visible absorption spectrum. The band gap width of the material is calculated using the Tauc plot method and extrapolating the straight-line part to the intersection of the abscissa. Atomic force microscopystudy (AFM) images were obtained using a Bruker Dimension Icon atomic force microscope.

4. Computational Methods

The structure optimizations were performed using the Gaussian 16 package[2], and the density functional theory (DFT) method B3LYP-D3 (with the default D3 dispersion correction proposed by Grimme)[3-5] with the 6-31G(d) basis-set.[6-8] To perfrom the quantum mechanics calculation for COF material, the model was constructed by extracting a unit from the COF material, and the boundaries of the truncated unit were capped with hydrogen atoms. Hybrid DFT methods, such as B3LYP, predict many of the electronic properties correctly, and it performs well for different properties of conjugated polymers, such as geometries and band gaps[9-12] The HOMO/LUMO and their energies were computed at the B3LYP-D3/6-31G(d) level. Structural modeling of COFs was generated using the BIOVIA Materials Studio[13] program employing the Building (Crystal) module, and the lattice model was geometrically optimized using force-filed based method (Forcite molecular dynamics module) and SCC-DFTB (DFTB + module). Pawley fitting (Reflex module) was performed iteratively to optimize the lattice parameters until the R_{wp} value converged and showed good agreement with the overlay of observed and refined profiles. Powder indexing and Rietveld refinement were performed using EXPO2014[14] various topology structures were illustrated using VESTA software[15].

5. Nonlinear optical measurements

The third-order nonlinear optical (NLO) properties of TF-BD and TFP-BD films were investigated using open-aperture Z-scan techniques. The laser used in the experiment was a mode-locked Nd:YAG laser at 532 nm. The ENERGY probe was Rj-7620 ENERGY RATIOMETER, with detection wavelength of 532 nm, pulse width of 4 ns, the laser pulse energy of 5-10 μJ, and focal spot beam waist radius of 30 μm. The glass sheet attached to the sample was placed on a mobile platform and used directly for testing. All testing procedures were conducted at room temperature. The sample moves in the direction of optical path propagation near the focal point of the lens, and the transmittance was monitored by two energy detectors.

Normalized transmittance higher than 1.0 will be observed when the sample exhibits saturable absorption (SA). In contrast, a normalized transmittance lower than 1.0 indicates that the sample has reverse saturated absorption (RSA)[16].

In addition, the nonlinear absorption coefficients (*β*) of TF-BD and TFP-BD films were fitted by the formula.

$$T = \frac{1}{\sqrt{\pi}\left[\beta I_0 L_{eff} \Big/ \left(1 + Z^2 \Big/ Z_0^2\right)\right]} \int_{-\infty}^{+\infty} \ln\left[1 + \frac{\beta I_0 L_{eff}}{\left(1 + \frac{Z^2}{Z_0^2}\right)} \exp\left(-t^2\right)\right] dt$$

Where T is normalized transmittance, I_0 is the input peak intensity at the focal point, and Z_0 is the Rayleigh diffraction length which can be calculated by $Z_0 = \pi\omega_0^2/\lambda$. λ is the wavelength, $L_{eff} = (1 - e^{-\alpha_0 L})/\alpha_0$. The thickness (L) in the fitting formula uses the COF films thickness measured by AFM. Since COF films are attached to both sides of the glass sheet during the preparation of COF films, the L used in the calculation of COFs *β* is twice the thickness of the film measured by the actual AFM.

Figures and Tables

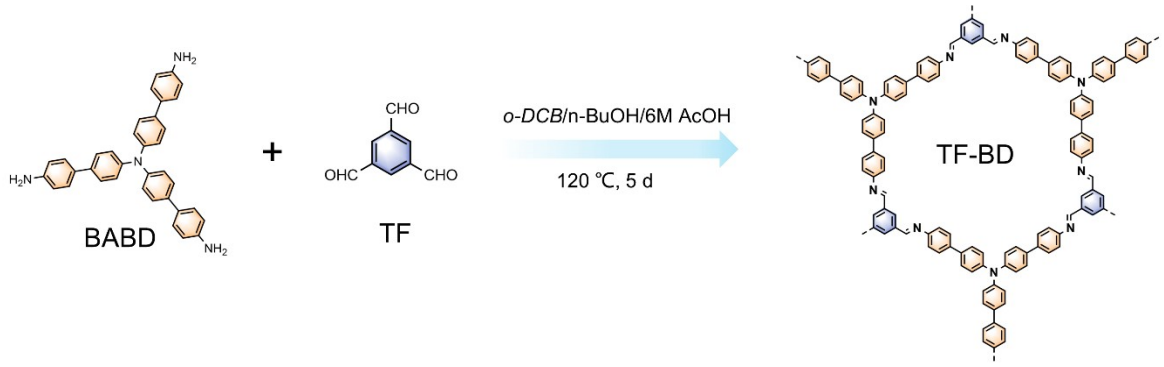

Scheme S1. Syntheses and structures of TF-BD.

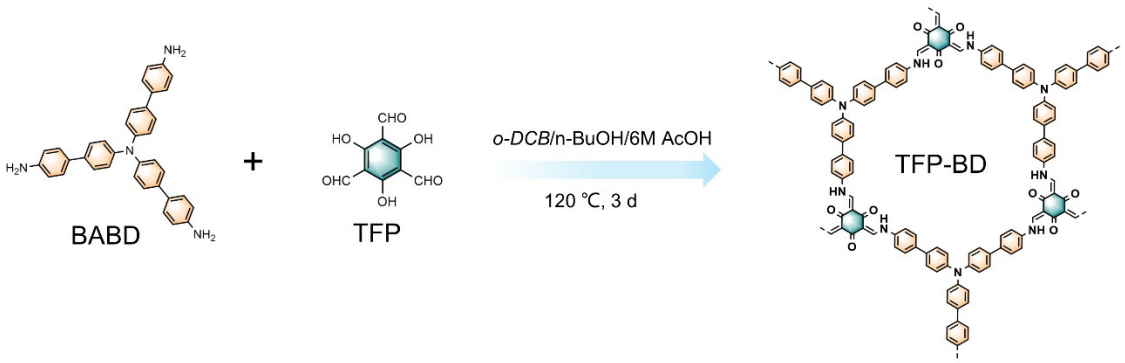

Scheme S2. Syntheses and structures of TFP-BD.

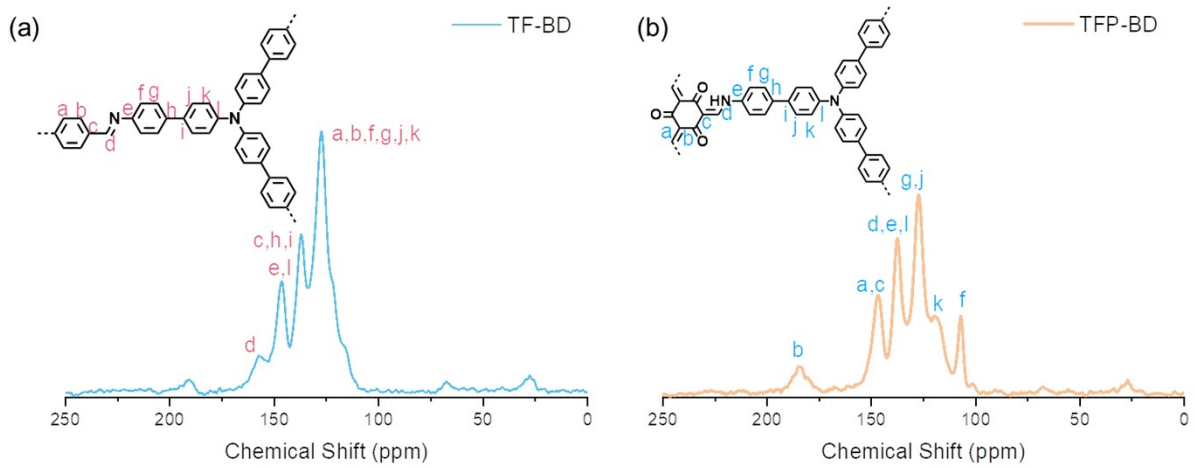

Figure S1. Solid-state CP-MAS ^{13}C NMR of (a) TF-BD and (b) TFP-BD.

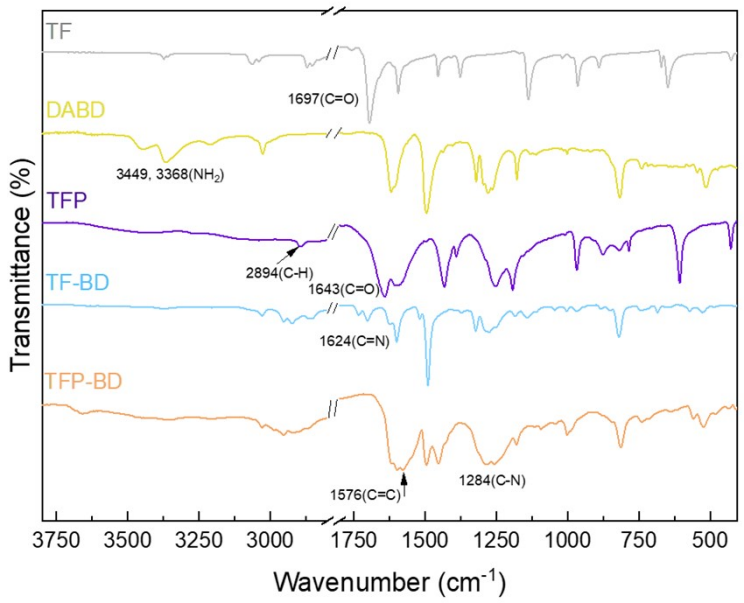

Figure S2. FT-IR spectra of TF, TFP, BABD, TF-BD, and TFP-BD.

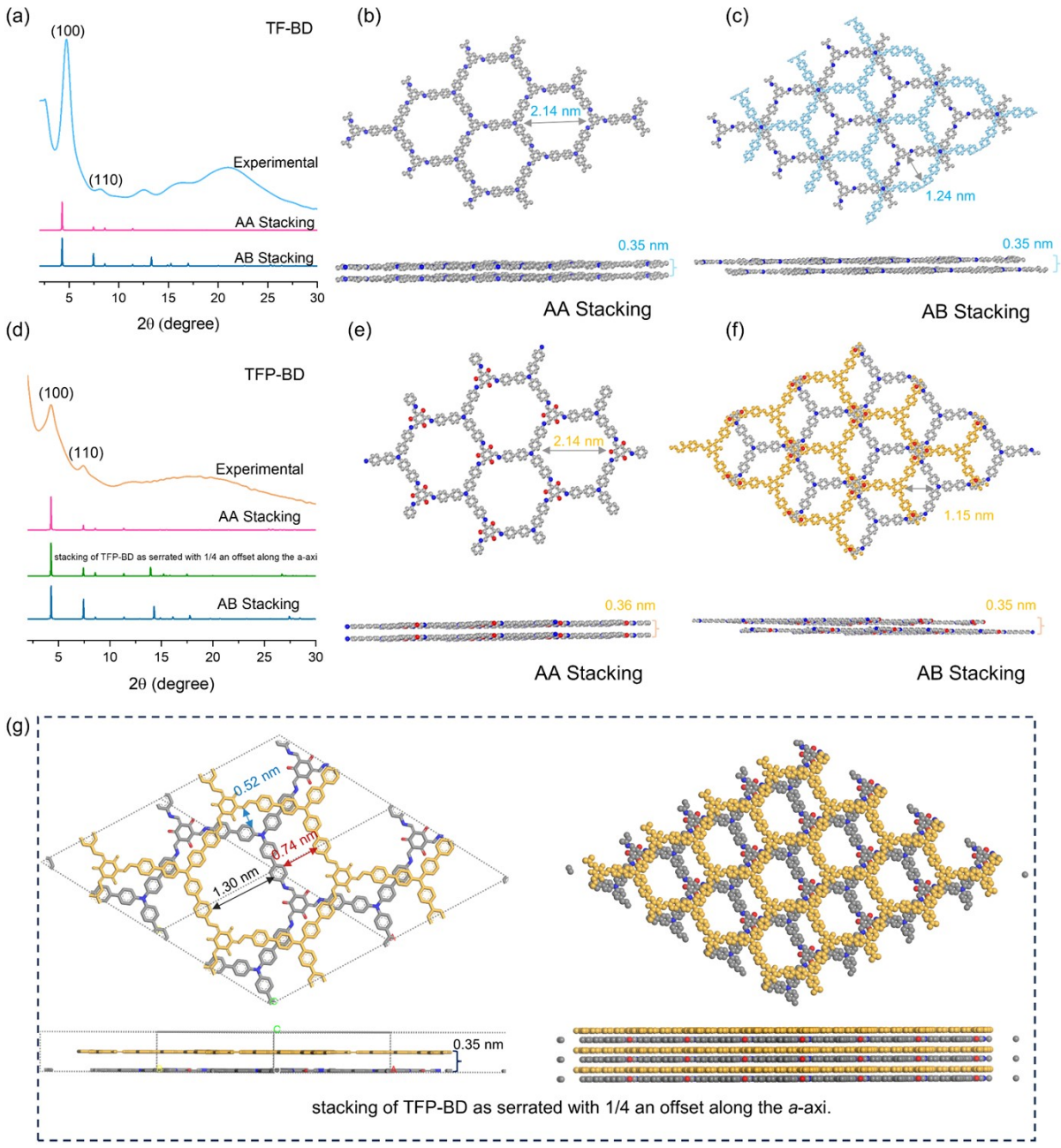

Figure S3. The top and side views of the structural model of COFs with eclipsed (AA) and staggered (AB) stacking (Gray: C; Blue: N; Red: O). (a) Experimental and simulated PXRD patterns for TF-BD. (b) AA stacking structure of TF-BD. (c) AB stacking structure of TF-BD. (d) Experimental and simulated PXRD patterns for TFP-BD. (e) AA stacking structure of TFP-BD. (f) AB stacking structure of TFP-BD. (g) stacking of TFP-BD as serrated with 1/4 an offset along the a-axi.

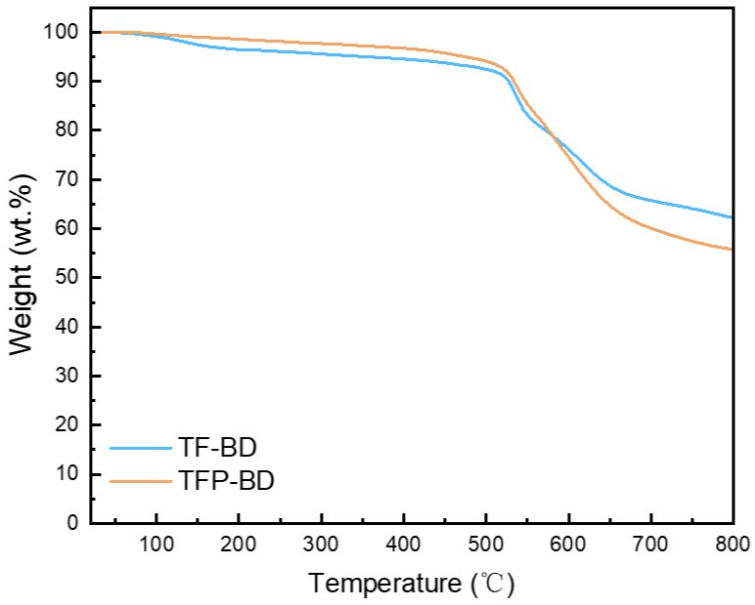

Figure S4. TGA curves of TF-BD and TFP-BD.

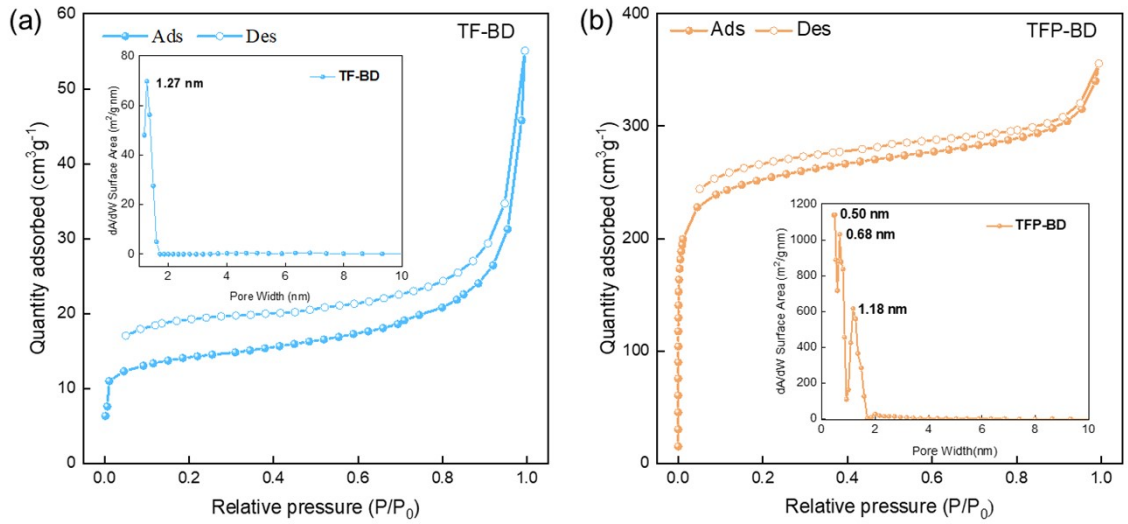

Figure S5. Nitrogen sorption isotherm of the (a) TF-BD and (b) TFP-BD measured at 77 K (Inset: Pore size distribution profile of the TF-BD and TFP-BD, respectively).

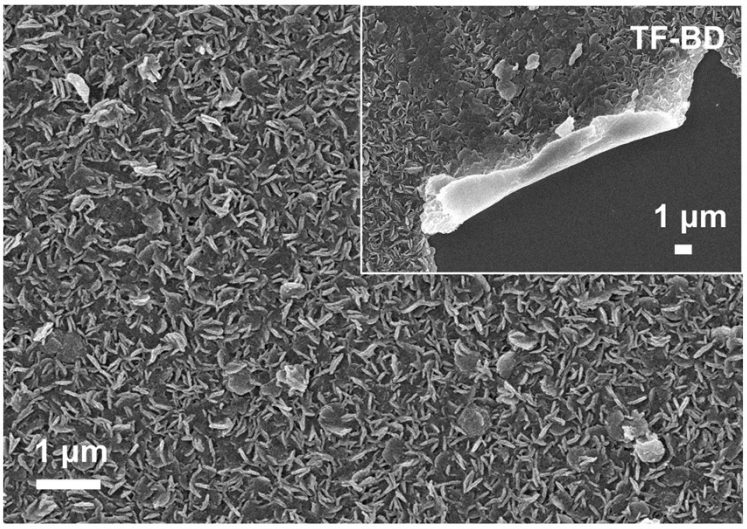

Figure S6. SEM images of TF-BD film.

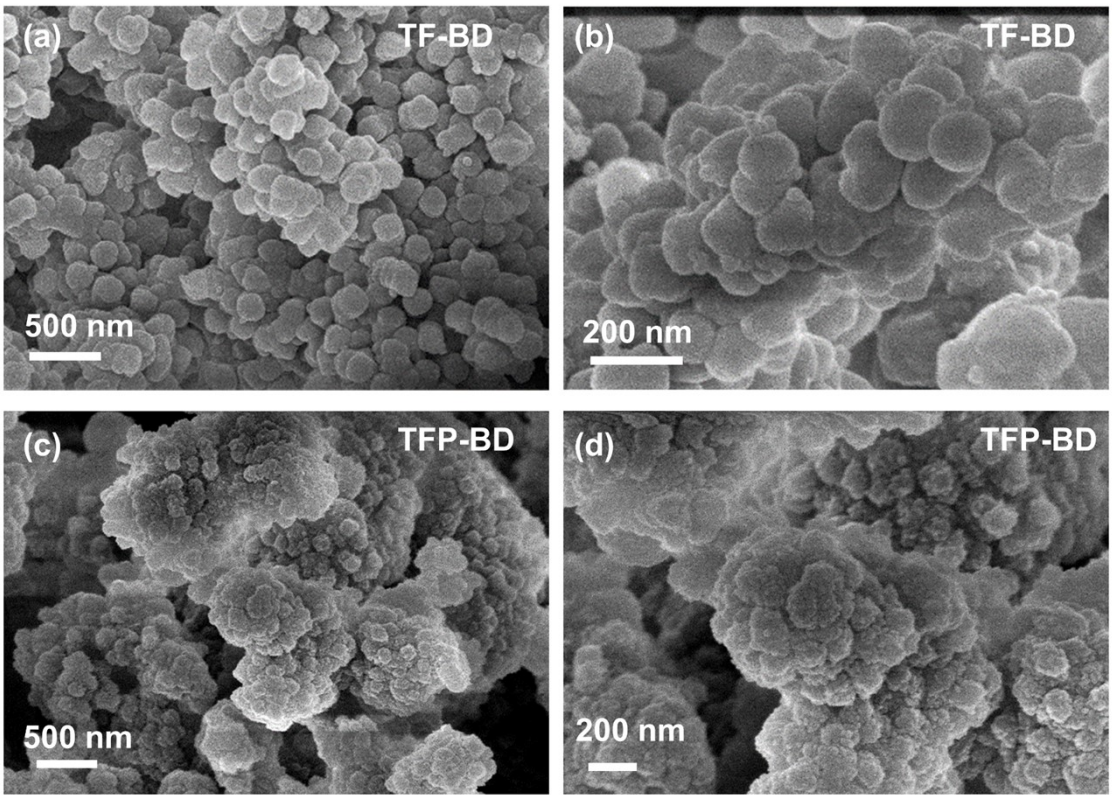

Figure S7. (a, b) SEM images of TF-BD powder, (c, d) SEM images of TFP-BD powder.

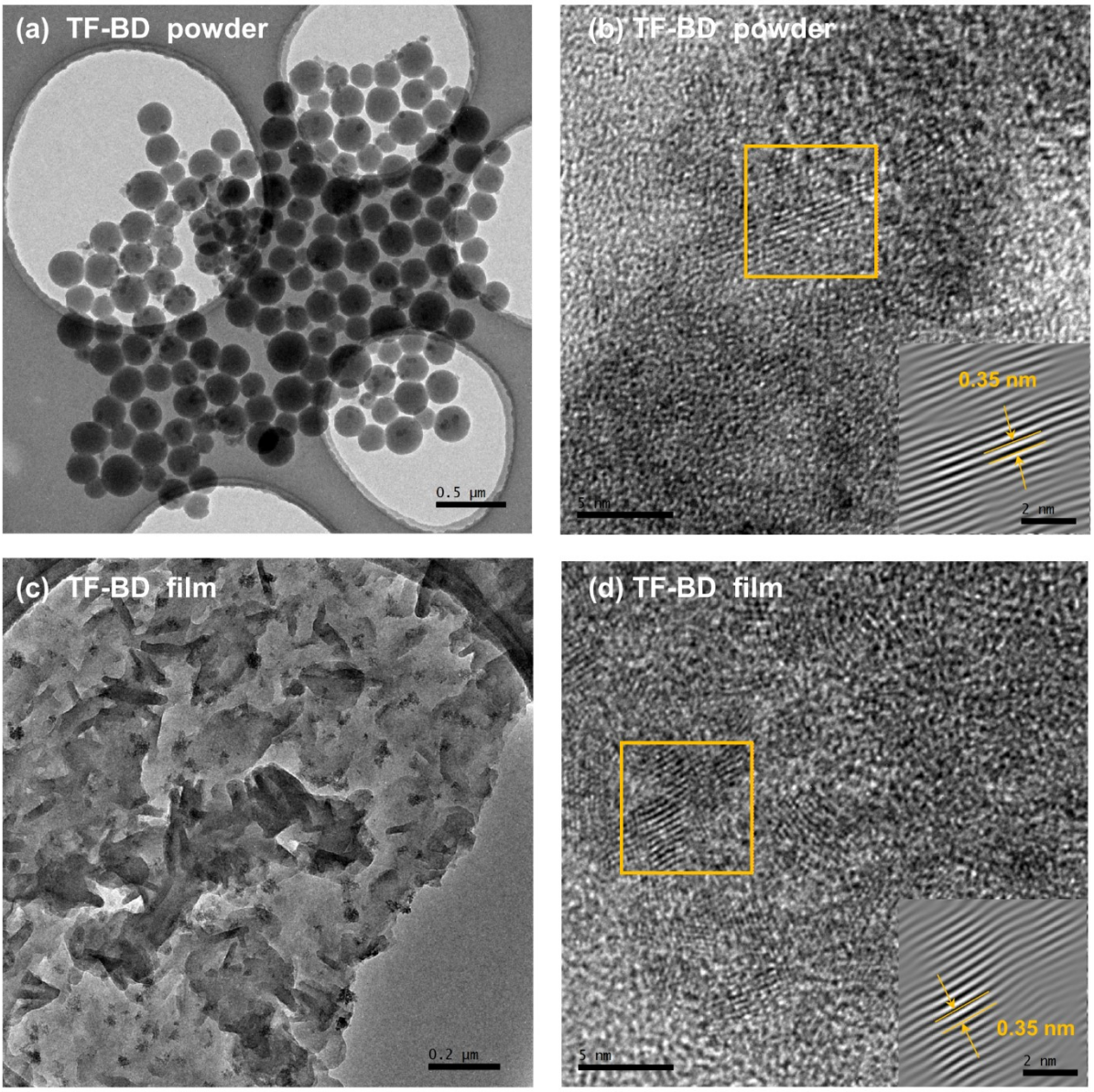

Figure S8. (a) TEM and (b) HR-TEM images of TF-BD powder. (c) TEM and (d) HR-TEM images of TF-BD film.

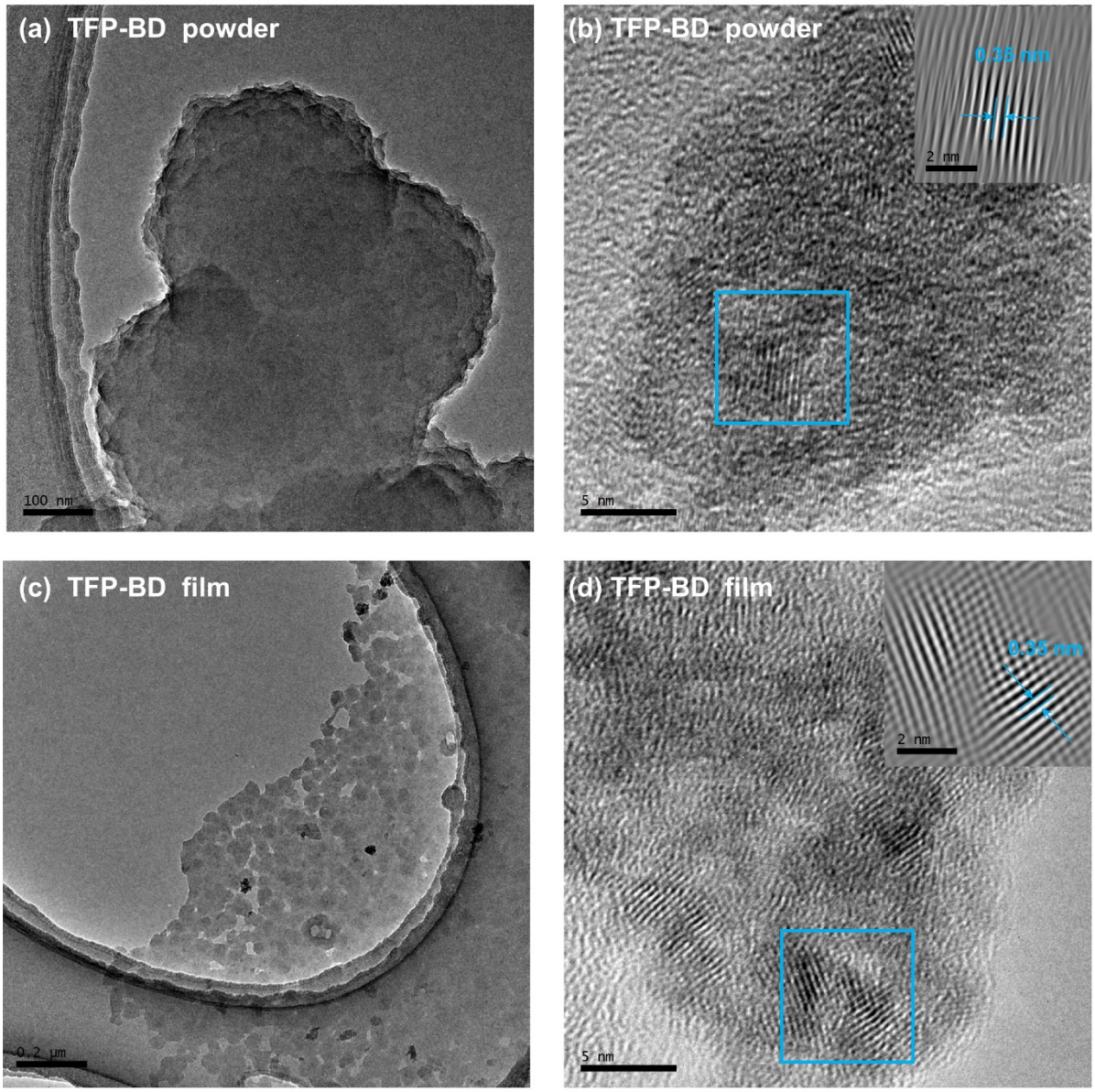

Figure S9. (a) TEM and (b) HR-TEM images of TFP-BD powder. (c) TEM and (d) HR-TEM images of TFP-BD film.

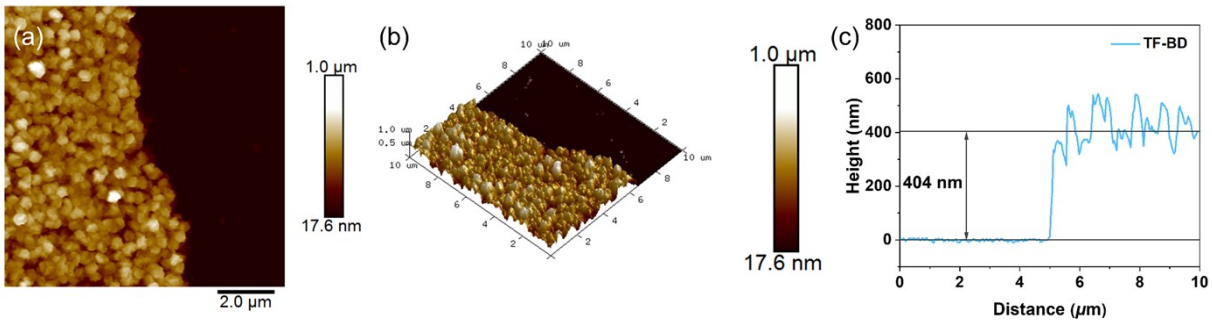

Figure S10. (a) AFM graph, (b) 3D graphs and (c) height profiles of TF-BD COF film.

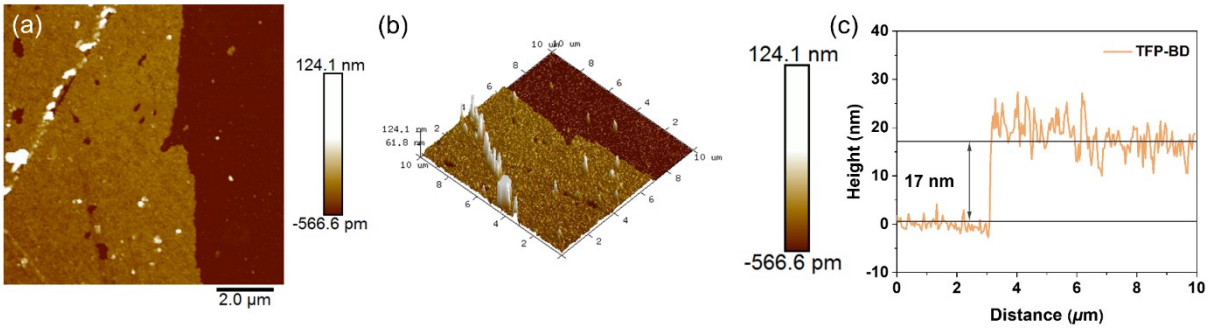

Figure S11. (a) AFM graph, (b) 3D graphs and (c) height profiles of TFP-BD COF film.

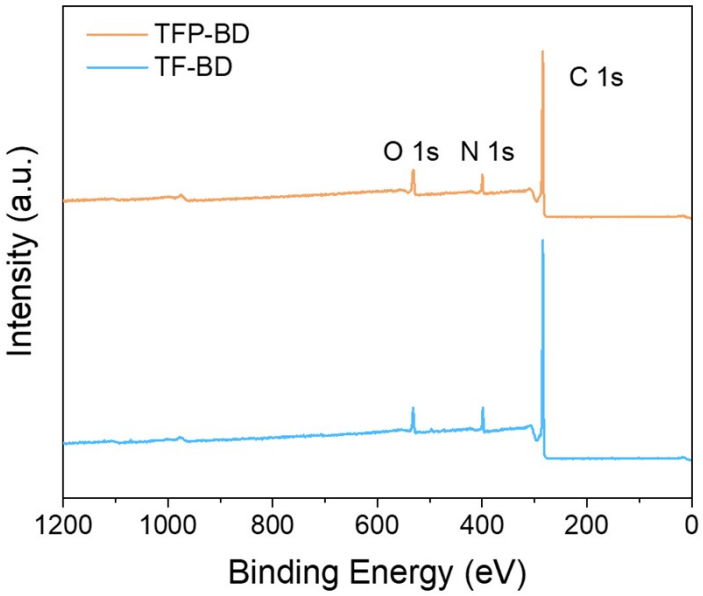

Figure S12. Survey XPS spectra of COF films.

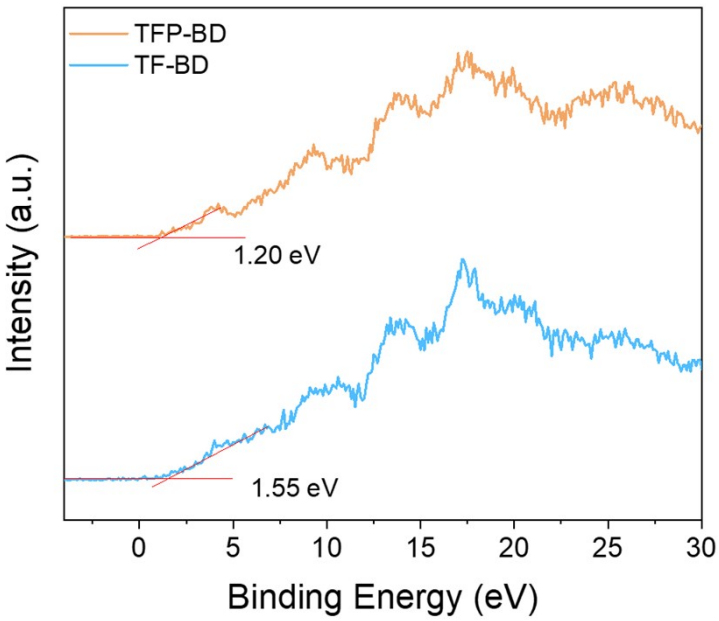

Figure S13. Valence-band XPS spectrum of TFP-BD and TF-BD COFs.

Table S1. Summary of the proportions of different elements in COFs by XPS analysis.

Sample	C (wt%)	N (wt%)	O (wt%)
TF-BD	87.55	6.96	5.49
TFP-BD	85.69	6.03	8.28

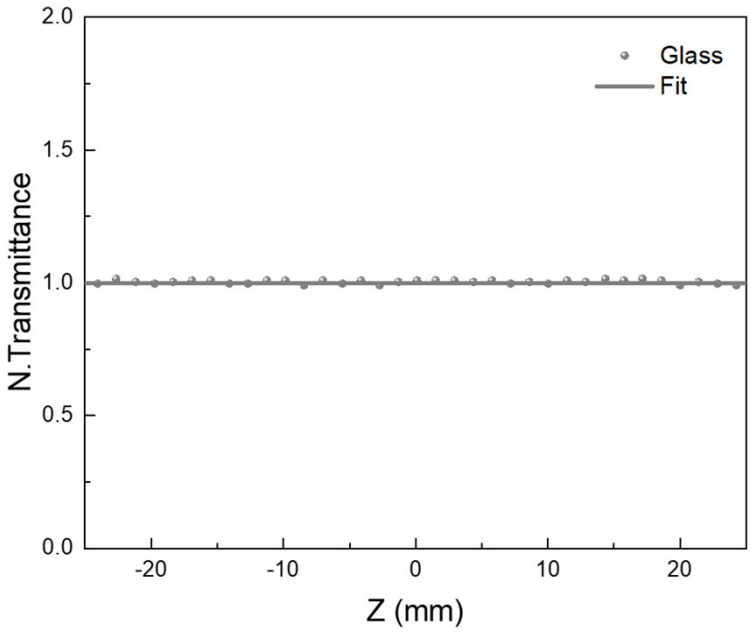

Figure S14. Open-aperture Z-scan curves of glass at pulse energy of 10 μJ.

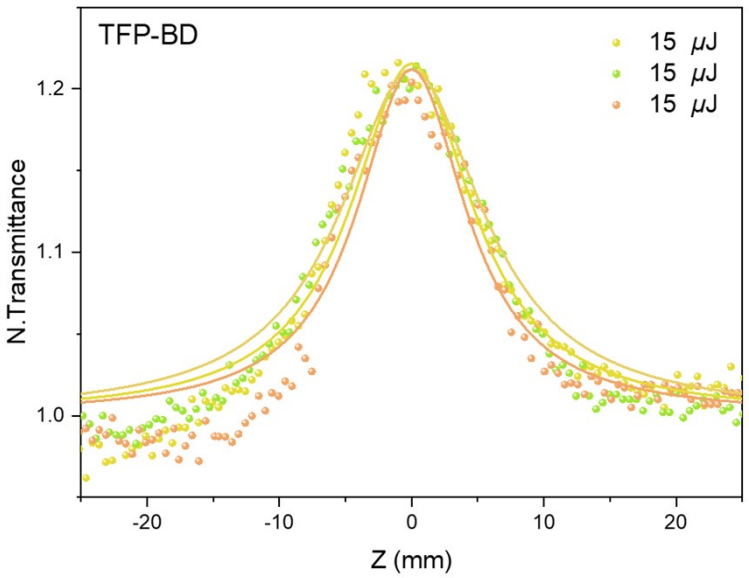

Figure S15. Open-aperture Z-scan curves with pulse energy of 15 μJ at the same position repeated 3 times of TFP-BD.

The third-order NLO stability of the prepared COFs film was further demonstrated by three experiments at the same position of TFP-BD film at 15 μJ (Fig. S15).

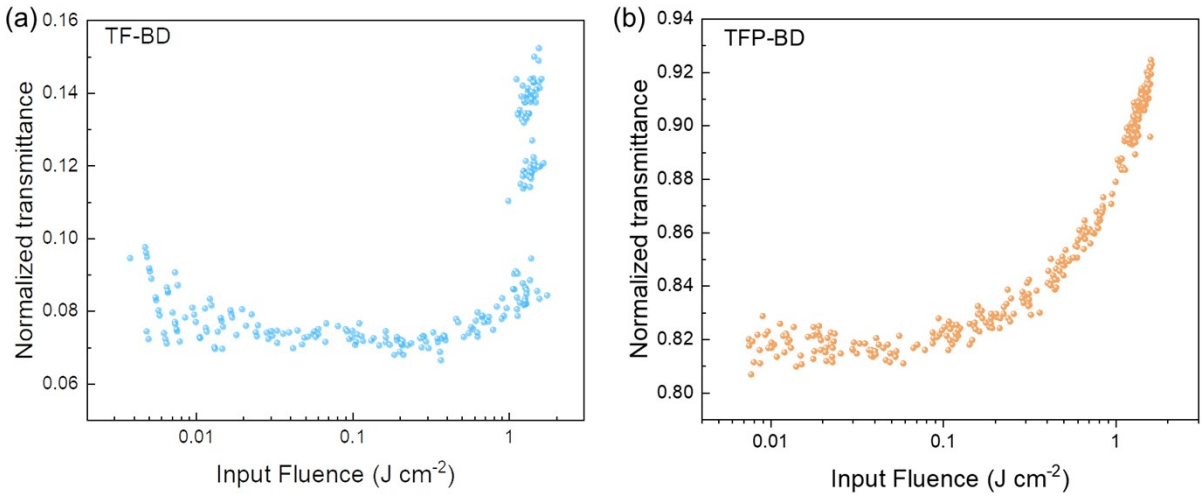

Figure S16. The plots of normalized transmittance versus input fluence (a) TF-BD and (b) TFP-BD films.

Table S2. Calculated HOMO energy level, LUMO energy level, and HOMO-LUMO gaps values of COF films in B3LYP/6-31G(d).

Sample	E_{HOMO} (eV)	E_{LUMO} (eV)	*HOMO-LUMO gaps* (eV)
TF-BD	−4.82	−1.63	3.19
TFP-BD	−5.00	−2.63	2.37

Table S3. Third order nonlinear optical refraction parameters of the COF films obtained with different pulse energies by open-aperture Z-scan.

Sample	Pulse energy (μJ)	Transmittance	L (nm)	L_{eff} (nm)	Fit depth	β (cm GW^{-1})
TF-BD	5	0.17	404	386	0.22	2.81×10^{4}
	10	0.18			0.45	-2.80×10^{4}
TFP-BD	5	0.73	17	29	0.40	-2.01×10^{5}
	10	0.73			1.00	-3.01×10^{5}
	15	0.73			0.61	-2.04×10^{5}
	15	0.73			0.60	-2.01×10^{5}
	15	0.73			0.60	-2.01×10^{5}

β: nonlinear absorption coefficient, negative (−) values represent saturation absorption.

Table S4. Comparison of nonlinear absorption coefficients (β, negative (−) values represent saturation absorption) of third-order nonlinear optical materials reported recently.

	Name	**Measurement condition**	**β (cm GW^{-1})**	**Ref.**
1	TFP-BD	Z-scan, 532 nm, 10 μJ	−3.01 × 10^5 cm GW^{-1}	***This work***
	TF-BD	Z-scan, 532 nm, 10 μJ	−2.80 × 10^4 cm GW^{-1}	***This work***
2	NOC6F-2/PMMA	Z-scan	7.2 × 10^{-10} m W^{-1}	17
3	MoS_2/graphene	Z-scan, 800 nm, I_0 ~ 123 GW cm^{-2}	−1217.8 cm GW^{-1}	18
5	$Cs_2AgBiBr_6$	Z-scan, 515 nm and 800 nm	(−2.0 ± 0.6) × 10^4 cm GW^{-1} (515 nm); (−7.1 ± 0.05) × 10^3 cm GW^{-1} (800 nm)	19
6	De-4.8	Z-scan, 800 nm	−1578 ± 49 cm GW^{-1}	20
7	Cu–Al–O thin films	Z-scan, 1550 nm	−6.29 × 10^{-5} cm W^{-1}	21
8	L3	Z-scan, 400 nm	−80.63 cm GW^{-1}	22
9	GaS	Z-scan, 800 nm; 1066 nm	–9.3 × 10^3 cm GW^{-1} (800 nm); −91 cm GW^{-1} (1066 nm)	23

10	BTFA nanofilm COF	Z-scan, 800 nm;	-10.1×10^3 cm GW^{-1}	24
11	MoS_2 film	Z-scan	-11.4 cm GW^{-1}	25
12	WS_2 film	Z-scan	-5.25×10^2 cm GW^{-1}	
13	Bi_2O_2Se	Z-scan	-2.9×10^3 cm GW^{-1}	26
14	$PtSe_2$	Z-scan	-9.94×10^3 cm GW^{-1}	27
15	BP	Z-scan	-0.01 cm GW^{-1}	28
16	BPQDs/PMMA	Z-scan	$-(0.41 \pm 0.06) \times 10^{-3}$ cm GW^{-1}	29
17	Mxene	Z-scan	-0.297 cm GW^{-1}	30
18	GDY-PVP nanocomposite	Z-scan	-10.96 cm GW^{-1}	31
19	GO	Z-scan	-40 cm GW^{-1}	32
20	$Ti_3C_2T_x$(=O rich)	515 nm	-1020 ± 136.2 cm GW^{-1}	33
21	HgL2-1.0–150	Z-scan, 532 nm, 11 μJ	-134 cm GW^{-1}	34

Table S5. Unit cell parameters and fractional atomic coordinates for TF-BD were calculated based on the AB stacking.

Space group				*P*1			
Calculated unit cell				a = 23.7405 Å, b = 23.7405 Å, c = 7.0428 Å $\alpha = \beta = 90°$, $\gamma = 120°$.			
Atoms	X	Y	Z	Atoms	X	Y	Z
C1	1.05411	0.00771	0.33780	C50	0.73759	0.3648	0.79700
C2	1.08596	-0.02494	0.27116	C51	0.76944	0.33215	0.73036
C3	1.15370	0.00482	0.27247	C52	0.83718	0.36191	0.73167
C4	1.19190	0.06886	0.33746	C53	0.87538	0.42595	0.79666
C5	1.16077	0.10213	0.40264	C54	0.84425	0.45922	0.86184
C6	1.09298	0.07174	0.40428	C55	0.77646	0.42883	0.86348
C7	1.26375	0.10074	0.33717	C56	0.94723	0.45783	0.79637
C8	1.29451	0.06409	0.30963	C57	0.97799	0.42118	0.76882
C9	0.36482	0.0952	0.30980	C58	0.04830	0.45229	0.76899
C10	0.40282	0.16224	0.33606	C59	0.08630	0.51933	0.79526
C11	0.37239	0.19923	0.36329	C60	0.05587	0.55632	0.82249
C12	1.30208	0.16803	0.36437	C61	0.98556	0.52512	0.82356
N13	0.47217	0.19149	0.33511	N62	0.15565	0.54858	0.79431
C14	0.58201	0.28169	0.34599	C63	0.26549	0.63878	0.80519
C15	0.61014	0.24198	0.34606	C64	0.29362	0.59907	0.80526
C16	0.51125	0.25375	0.34608	C65	0.19473	0.61084	0.80527
C17	0.95172	0.01570	0.33780	C66	0.63520	0.37279	0.79700
C18	0.98437	0.08020	0.27116	C67	0.66785	0.43729	0.73036
C19	0.95461	0.11818	0.27247	C68	0.63809	0.47527	0.73167
C20	0.89057	0.09234	0.33746	C69	0.57405	0.44943	0.79666
C21	0.85730	0.02794	0.40264	C70	0.54078	0.38503	0.86184
C22	0.88769	-0.00946	0.40428	C71	0.57117	0.34763	0.86348
C23	0.85869	0.13231	0.33717	C72	0.54217	0.48940	0.79637
C24	0.89534	0.19972	0.30963	C73	0.57882	0.55681	0.76882

C25	0.86423	0.23892	0.3098	C74	0.54771	0.59601	0.76899
C26	0.79719	0.20988	0.33606	C75	0.48067	0.56697	0.79526
C27	0.76020	0.14246	0.36329	C76	0.44368	0.49955	0.82249
C28	0.79140	0.10335	0.36437	C77	0.47488	0.46044	0.82356
N29	0.76794	0.24998	0.33511	N78	0.45142	0.60707	0.79431
C30	0.67774	0.26962	0.34599	C79	0.36122	0.62671	0.80519
C31	0.71745	0.33746	0.34606	C80	0.40093	0.69455	0.80526
C32	0.70568	0.22680	0.34608	C81	0.38916	0.58389	0.80527
C33	0.94373	-0.09468	0.33780	C82	0.62721	0.26241	0.79700
C34	0.87923	-0.12653	0.27116	C83	0.56271	0.23056	0.73036
C35	0.84125	-0.19427	0.27247	C84	0.52473	0.16282	0.73167
C36	0.86709	-0.23247	0.33746	C85	0.55057	0.12462	0.79666
C37	0.93149	-0.20134	0.40264	C86	0.61497	0.15575	0.86184
C38	0.96889	-0.13355	0.40428	C87	0.65237	0.22354	0.86348
C39	0.82712	-0.30432	0.33717	C88	0.51060	0.05277	0.79637
C40	0.75971	-0.33508	0.30963	C89	0.44319	0.02201	0.76882
C41	0.72051	0.59461	0.3098	C90	0.40399	0.95170	0.76899
C42	0.74955	0.55661	0.33606	C91	0.43303	0.91370	0.79526
C43	0.81697	0.58704	0.36329	C92	0.50045	0.94413	0.82249
C44	0.85608	-0.34265	0.36437	C93	0.53956	0.01444	0.82356
N45	0.70945	0.48726	0.33511	N94	0.39293	0.84435	0.79431
C46	0.68981	0.37742	0.34599	C95	0.37329	0.73451	0.80519
C47	0.62197	0.34929	0.34606	C96	0.30545	0.70638	0.80526
C48	0.73263	0.44818	0.34608	C97	0.41611	0.80527	0.80527
N49	0.98319	-0.02376	0.33788	N98	0.66667	0.33333	0.79707

Table S6. Unit cell parameters and fractional atomic coordinates for TFP-BD were calculated based on the AB stacking.

Space group				*P*1			
Calculated unit cell				*a* = 23.8228 Å, *b* = 23.8228 Å, *c* = 7.0200 Å *α* = *β* = 90°, *γ* = 120°.			
Atoms	X	Y	Z	Atoms	X	Y	Z
C1	0.74307	0.48185	0.31371	C53	0.07896	0.15159	-0.27071
C2	0.81164	0.52501	0.31371	C54	0.14750	0.19465	-0.27071
C3	0.83992	0.59396	0.31371	C55	0.17576	0.26354	-0.27071
C4	0.90742	0.63310	0.31371	C56	0.24323	0.30265	-0.27071
C5	0.93605	0.70064	0.31371	C57	0.27183	0.37018	-0.27071
C6	0.89750	0.73000	0.31371	C58	0.23329	0.39958	-0.27071
C7	0.82975	0.69036	0.31371	C59	0.16554	0.35991	-0.27071
C8	0.80115	0.62293	0.31371	C60	0.13697	0.29248	-0.27071
C9	0.71534	0.41694	0.31371	C61	0.0513	0.08674	-0.27071
C10	0.75368	0.38318	0.31371	C62	0.0897	0.05309	-0.27071
C11	0.92758	0.80151	0.31371	C63	0.26342	0.47116	-0.27071
C12	0.99497	0.84148	0.31371	C64	0.33083	0.51116	-0.27071
N13	0.02269	0.90881	0.31371	N65	0.35863	0.57855	-0.27071
C14	0.98537	0.93974	0.31371	C66	0.32136	0.60956	-0.27071
C15	0.91767	0.89797	0.31371	C67	0.25364	0.56778	-0.27071
C16	0.88909	0.8306	0.31371	C68	0.22500	0.50034	-0.27071
O17	0.61230	0.40605	0.31371	O69	0.94829	0.07581	-0.27071
C18	0.54492	0.26886	0.31371	C70	0.88112	0.93870	-0.27071
C19	0.50176	0.29427	0.31371	C71	0.83806	0.96418	-0.27071
C20	0.43281	0.25360	0.31371	C72	0.76917	0.92355	-0.27071
C21	0.39367	0.28196	0.31371	C73	0.73006	0.95191	-0.27071
C22	0.32613	0.24305	0.31371	C74	0.66253	0.91298	-0.27071
C23	0.29677	0.17514	0.31371	C75	0.63313	0.84504	-0.27071
C24	0.33641	0.14703	0.31371	C76	0.6728	0.81696	-0.27071
C25	0.40384	0.18586	0.31371	C77	0.74023	0.85582	-0.27071

C26	0.60983	0.30604	0.31371	C78	0.94597	0.97589	-0.27071
C27	0.64359	0.37814	0.31371	C79	0.97962	0.04794	-0.27071
C28	0.22526	0.13371	0.31371	C80	0.56155	0.80359	-0.27071
C29	0.18529	0.16113	0.31371	C81	0.52155	0.831	-0.27071
N30	0.11796	0.12152	0.31371	N82	0.45416	0.79141	-0.27071
C31	0.08703	0.05327	0.31371	C83	0.42315	0.72313	-0.27071
C32	0.1288	0.02734	0.31371	C84	0.46493	0.69719	-0.27071
C33	0.19617	0.06613	0.31371	C85	0.53237	0.73599	-0.27071
O34	0.62072	0.21389	0.31371	O86	0.9569	0.88381	-0.27071
C35	0.75791	0.2837	0.31371	C87	0.09401	0.95375	-0.27071
C36	0.7325	0.21513	0.31371	C88	0.06853	0.88521	-0.27071
C37	0.77317	0.18685	0.31371	C89	0.10916	0.85695	-0.27071
C38	0.74481	0.11935	0.31371	C90	0.0808	0.78948	-0.27071
C39	0.78372	0.09072	0.31371	C91	0.11973	0.76088	-0.27071
C40	0.85163	0.12927	0.31371	C92	0.18767	0.79942	-0.27071
C41	0.87974	0.19702	0.31371	C93	0.21575	0.86717	-0.27071
C42	0.84091	0.22562	0.31371	C94	0.17689	0.89574	-0.27071
C43	0.72073	0.31143	0.31371	C95	0.05682	0.98141	-0.27071
C44	0.64863	0.27309	0.31371	C96	0.98477	0.94301	-0.27071
C45	0.89306	0.09919	0.31371	C97	0.22912	0.76929	-0.27071
C46	0.86564	0.0318	0.31371	C98	0.20171	0.70188	-0.27071
N47	0.90525	1.00408	0.31371	N99	0.24130	0.67408	-0.27071
C48	0.97350	0.04140	0.31371	C100	0.30958	0.71135	-0.27071
C49	0.99943	0.1091	0.31371	C101	0.33552	0.77907	-0.27071
C50	0.96064	0.13768	0.31371	C102	0.29672	0.80771	-0.27071
O51	0.81288	0.41447	0.31371	O103	0.14890	0.08442	-0.27071
N52	0.01530	0.01147	0.31371	N104	0.35137	0.68135	-0.27071

References

1. M. Li, C. Gong, J. Du, D. Ding, D. Du, D. Wang, J. Jiang, T. Li, C. Zheng, Y.-F. Yang, Y. She and J. Jia, Donor–Acceptor Covalent Organic Frameworks Films with Ultralow Band Gaps to Enhanced Third-Order Nonlinear Optical Properties, *ACS Materials Lett.*, 2023, **5**, 694-703.
2. M. J. Frisch, G. W. Trucks, H. B. Schlegel, G. E. Scuseria, M. A. Robb, J. R. Cheeseman, G. Scalmani, V. Barone, G. A. Petersson, H. Nakatsuji, X. Li, M. Caricato, A. V. Marenich, J. Bloino, B. G. Janesko, R. Gomperts, B. Mennucci, H. P. Hratchian, J. V. Ortiz, A. F. Izmaylov, J. L. Sonnenberg, Williams, F. Ding, F. Lipparini, F. Egidi, J. Goings, B. Peng, A. Petrone, T. Henderson, D. Ranasinghe, V. G. Zakrzewski, J. Gao, N. Rega, G. Zheng, W. Liang, M. Hada, M. Ehara, K. Toyota, R. Fukuda, J. Hasegawa, M. Ishida, T. Nakajima, Y. Honda, O. Kitao, H. Nakai, T. Vreven, K. Throssell, J. A. Montgomery Jr., J. E. Peralta, F. Ogliaro, M. J. Bearpark, J. J. Heyd, E. N. Brothers, K. N. Kudin, V. N. Staroverov, T. A. Keith, R. Kobayashi, J. Normand, K. Raghavachari, A. P. Rendell, J. C. Burant, S. S. Iyengar, J. Tomasi, M. Cossi, J. M. Millam, M. Klene, C. Adamo, R. Cammi, J. W. Ochterski, R. L. Martin, K. Morokuma, O. Farkas, J. B. Foresman and D. J. Fox, Gaussian 16 Rev. A.03.*Journal*, 2016.
3. A. D. Becke, A new mixing of Hartree–Fock and local density-functional theories, *J. Chem. Phys.*, 1993, **98**, 1372-1377.
4. A. D. Becke, Density-functional thermochemistry. III. The role of exact exchange, *J. Chem. Phys.*, 1993, **98**, 5648-5652.
5. P. J. Stephens, F. J. Devlin, C. F. Chabalowski and M. J. Frisch, Ab Initio Calculation of Vibrational Absorption and Circular Dichroism Spectra Using Density Functional Force Fields, *J. Phys. Chem.*, 1994, **98**, 11623-11627.
6. R. Ditchfield, W. J. Hehre and J. A. Pople, Self-Consistent Molecular-Orbital Methods. IX. An Extended Gaussian-Type Basis for Molecular-Orbital Studies of Organic Molecules, *J. Chem. Phys.*, 1971, **54**, 724-728.
7. W. J. Hehre, R. Ditchfield and J. A. Pople, Self—Consistent Molecular Orbital Methods. XII. Further Extensions of Gaussian—Type Basis Sets for Use in Molecular Orbital Studies of Organic Molecules, *J. Chem. Phys.*, 1972, **56**, 2257-2261.
8. S. Manzetti and T. Lu, Alternant conjugated oligomers with tunable and narrow HOMO-LUMO gaps as sustainable nanowires, *RSC Adv.*,

2013, **3**, 25881-25890.
9. Z. Qiao, H. Han, X. Li, X. Wang, T. Lan, R. Wang and W. Ji, Dual Functional sp^2 Carbon-Conjugated Nanoporous Covalent Organic Framework as a Janus Fluorescence Sensor for the Detection of Hazardous Substances, *ACS Appl. Nano Mater.*, 2022, **5**, 11465-11473.
10. X. Chen, H. Zhang, C. Ci, W. Sun and Y. Wang, Few-Layered Boronic Ester Based Covalent Organic Frameworks/Carbon Nanotube Composites for High-Performance K-Organic Batteries, *ACS Nano*, 2019, **13**, 3600-3607.
11. C. Zhang, S. Zhang, Y. Yan, F. Xia, A. Huang and Y. Xian, Highly Fluorescent Polyimide Covalent Organic Nanosheets as Sensing Probes for the Detection of 2,4,6-Trinitrophenol, *ACS Appl. Mater. Interfaces*, 2017, **9**, 13415-13421.
12. R. Xia, X. Zheng, C. Li, X. Yuan, J. Wang, Z. Xie and X. Jing, Nanoscale Covalent Organic Frameworks with Donor–Acceptor Structure for Enhanced Photothermal Ablation of Tumors, *ACS Nano*, 2021, **15**, 7638-7648.
13. Materials Studio; Accelrys: San Diego.
14. http://www.ba.ic.cnr.it/softwareic/expo/.
15. http://www.jp-minerals.org/vesta/en/.
16. L. Xu, J. Sun, T. Tang, H. Zhang, M. Sun, J. Zhang, J. Li, B. Huang, Z. Wang, Z. Xie and W. Y. Wong, Metallated Graphynes as a New Class of Photofunctional 2D Organometallic Nanosheets, *Angew. Chem. Int. Ed.*, 2021, **60**, 11326-11334.
17. T. Dong, J. Li, C. Wang, L. Yu, Y. Song, C. Wang, L. Jiang and C. Bai, Unexpected Third-Order Nonlinear Optical Responses in Two Isomeric Non-Fused Ring A-D-A Electron-Acceptor Molecules, *Adv. Optical Mater.*, 2023, **n/a**, 2300482.
18. M. He, C. Quan, C. He, Y. Huang, L. Zhu, Z. Yao, S. Zhang, J. Bai and X. Xu, Enhanced Nonlinear Saturable Absorption of MoS_2/Graphene Nanocomposite Films, *J. Phys. Chem. C*, 2017, **121**, 27147-27153.
19. B. Li, H. Li, Y. Sun, M. G. Humphrey, C. Zhang and Z. Huang, Defect-Dependent Nonlinear Absorption in the Lead-Free Double-Perovskite $Cs_2AgBiBr_6$, *ACS Appl. Mater. Interfaces*, 2023, **15**, 10858-10867.
20. Y. Sun, H. Li, X. Gao, M. G. Humphrey, C. Zhang and Z. Huang, Promoting the nonlinear optical absorption of conjugated polymers by in-gap states modulation via chemical dedoping, *Mat. Today Phys.*,

2023, **32**, 101024.
21. J. Xu, Q. Liu, X. Li, R. Hong, C. Tao, Q. Wang, H. Lin, Z. Han and D. Zhang, Tunability of nonlinear optical properties of amorphous Cu–Al–O films induced by thermal oxidation, *Opt. Mater.*, 2023, **136**, 113466.
22. X. Xiao, M. Liu, J. Zhou, H. Zhu, C. Wang, Z. Chen, Y. Wang, S. Xiao and J. He, The ultrafast tunable saturable absorption of three azo-Schiff base ligands and related metal complexes, *Opt. Mater.*, 2022, **132**, 112773.
23. S. Ahmed, P. K. Cheng, J. Qiao, W. Gao, A. M. Saleque, M. N. Al Subri Ivan, T. Wang, T. I. Alam, S. U. Hani, Z. L. Guo, S. F. Yu and Y. H. Tsang, Nonlinear Optical Activities in Two-Dimensional Gallium Sulfide: A Comprehensive Study, *ACS Nano*, 2022, **16**, 12390-12402.
24. Y. Luo, M. Li, J. Tang, J. Zang, Y. Wang, T. Liu and Y. Fang, Interfacially confined preparation of fumaronitrile-based nanofilms exhibiting broadband saturable absorption properties, *J. Colloid Interface Sci.*, 2022, **627**, 569-577.
25. S. Zhang, N. Dong, N. McEvoy, M. O'Brien, S. Winters, N. C. Berner, C. Yim, Y. Li, X. Zhang, Z. Chen, L. Zhang, G. S. Duesberg and J. Wang, Direct Observation of Degenerate Two-Photon Absorption and Its Saturation in WS_2 and MoS_2 Monolayer and Few-Layer Films, *ACS Nano*, 2015, **9**, 7142-7150.
26. X. Tian, H. Luo, R. Wei, C. Zhu, Q. Guo, D. Yang, F. Wang, J. Li and J. Qiu, An Ultrabroadband Mid-Infrared Pulsed Optical Switch Employing Solution-Processed Bismuth Oxyselenide, *Adv. Mater.*, 2018, **30**, 1801021.
27. G. Wang, Z. Wang, N. McEvoy, P. Fan and W. J. Blau, Layered PtSe2 for Sensing, Photonic, and (Opto-)Electronic Applications, *Adv. Mater.*, 2021, **33**, 2004070.
28. K. Wang, B. M. Szydłowska, G. Wang, X. Zhang, J. J. Wang, J. J. Magan, L. Zhang, J. N. Coleman, J. Wang and W. J. Blau, Ultrafast Nonlinear Excitation Dynamics of Black Phosphorus Nanosheets from Visible to Mid-Infrared, *ACS Nano*, 2016, **10**, 6923-6932.
29. Y. Xu, W. Wang, Y. Ge, H. Guo, X. Zhang, S. Chen, Y. Deng, Z. Lu and H. Zhang, Stabilization of Black Phosphorous Quantum Dots in PMMA Nanofiber Film and Broadband Nonlinear Optics and Ultrafast Photonics Application, *Adv. Funct. Mater.*, 2017, **27**, 1702437.
30. X. Jiang, S. Liu, W. Liang, S. Luo, Z. He, Y. Ge, H. Wang, R. Cao, F. Zhang, Q. Wen, J. Li, Q. Bao, D. Fan and H. Zhang, Broadband Nonlinear

Photonics in Few-Layer MXene Ti_3C_2Tx (T = F, O, or OH), *Laser Photonics Rev.*, 2018, **12**, 1700229.

31. J. Guo, R. Shi, R. Wang, Y. Wang, F. Zhang, C. Wang, H. Chen, C. Ma, Z. Wang, Y. Ge, Y. Song, Z. Luo, D. Fan, X. Jiang, J. Xu and H. Zhang, Graphdiyne-Polymer Nanocomposite as a Broadband and Robust Saturable Absorber for Ultrafast Photonics, *Laser Photonics Rev.*, 2020, **14**, 1900367.
32. S. Kumar, M. Anija, N. Kamaraju, K. S. Vasu, K. S. Subrahmanyam, A. K. Sood and C. N. R. Rao, Femtosecond carrier dynamics and saturable absorption in graphene suspensions, *Appl. Phys. Lett.*, 2009, **95**, 191911.
33. H. Li, S. Chen, D. W. Boukhvalov, Z. Yu, M. G. Humphrey, Z. Huang and C. Zhang, Switching the Nonlinear Optical Absorption of Titanium Carbide MXene by Modulation of the Surface Terminations, *ACS Nano*, 2022, **16**, 394-404.
34. L. Xu, J. Sun, T. Tang, H. Zhang, M. Sun, J. Zhang, J. Li, B. Huang, Z. Wang, Z. Xie and W.-Y. Wong, Metallated Graphynes as a New Class of Photofunctional 2D Organometallic Nanosheets, *Angew. Chem. Int. Ed.*, 2021, **60**, 11326-11334.